

A Family of Barycentric Coordinates for Co-Dimension 1 Manifolds with Simplicial Facets

Z. Yan¹ and S. Schaefer¹

¹Texas A&M University, College Station, USA

Abstract

We construct a family of barycentric coordinates for 2D shapes including non-convex shapes, shapes with boundaries, and skeletons. Furthermore, we extend these coordinates to 3D and arbitrary dimension. Our approach modifies the construction of the Floater-Hormann-Kós family of barycentric coordinates for 2D convex shapes. We show why such coordinates are restricted to convex shapes and show how to modify these coordinates to extend to discrete manifolds of co-dimension 1 whose boundaries are composed of simplicial facets. Our coordinates are well-defined everywhere (no poles) and easy to evaluate. While our construction is widely applicable to many domains, we show several examples related to image and mesh deformation.

CCS Concepts

• **Computing methodologies** → *Shape modeling; Parametric curve and surface models;*

1. Introduction

Barycentric coordinates are a fundamental tool in Computer Graphics. These coordinates are used in a wide variety of applications ranging from finite elements [Wac75; Wac81; MD04; SM06] to interpolation [FS08], parameterization [FH05], image warping [MJBF02], mesh deformation [JSWD05; LKCL07; ZDL*14] and image cloning [FHL*09].

Barycentric coordinates express the location of points in Euclidean space as linear combinations of a fixed set of vertices. Given a set of non-degenerate vertices of an n -gon $\{P_1, \dots, P_n\} \in \mathbb{R}^2$ with $n \geq 3$, we can write any point X on the plane as a linear combination of the P_i with coefficients $\{\lambda_1, \dots, \lambda_n\}$:

$$X = \sum_{i=1}^n \lambda_i P_i, \quad \sum_{i=1}^n \lambda_i = 1. \quad (1)$$

The coefficients λ_i are called the *generalized barycentric coordinates* [Flo15] of X when $n > 3$. Note that this equation implies that if we apply the λ_i to samples of a constant or linear function sampled at the P_i , these coordinates reproduce that sampled function. We refer to such a property as *linear precision*.

We can also rewrite Equation 1 in homogeneous form

$$\sum_{i=1}^n w_i (P_i - X) = 0, \quad \sum_{i=1}^n w_i \neq 0, \quad (2)$$

where $\lambda_i = \frac{w_i}{\sum_{i=1}^n w_i}$. Here the $\{w_i\}$ are called *homogeneous coordinates*.

Barycentric coordinates are not unique if $n > 3$, and each co-

ordinate w_i is a function of the point X as well as the P_i . Despite the lack of uniqueness, barycentric coordinates still must satisfy several geometric constraints. **Interpolation.** As X approaches a facet f^k on the boundary polygon with vertices P_i , then the $\lambda_j \rightarrow 0$ for all $P_j \notin f^k$. This property, along with the linear precision, implies that the barycentric coordinates approach the barycentric coordinates of the lower dimensional facet. In 2D, this implication means that the barycentric coordinates for points on edges reduce to 1D barycentric coordinates. **Partition of Unity.** Barycentric coordinates sum to 1 as shown in Equation 1 implying the reproduction of constant functions. **Non-negative.** Ideally, the coordinates λ_i should be greater than or equal to zero. However, few barycentric coordinate constructions achieve this property, particularly for non-convex shapes.

In this paper, we modified the construction of the Floater-Hormann-Kós family of barycentric coordinates for 2D convex shapes [FHK06]. We show why these coordinates were originally restricted to convex shapes, and we propose a modification to generalize this family of coordinates to non-convex polygons, shapes with boundaries, and even skeletons. We extend these coordinates to 3D, which provides a construction to generalize this family of coordinates to arbitrary dimension. Our coordinates are well-defined everywhere (no poles) and easy to evaluate.

2. Related Work

Barycentric coordinates that satisfy our desired properties for a simplex are unique. However these coordinates are not unique for

arbitrary polygons or polytopes. Hence, many kinds of coordinates have been developed. See [Flo15] for a survey on generalized barycentric coordinates.

Wachspress [Wac75] developed a generalization of barycentric coordinates to planar convex polygons for use in finite element applications. Warren [War96; War03] and Dasgupta [Das03] generalized Wachspress' original coordinates to convex polytopes in higher dimension Euclidean spaces [WSHD07; Wac11]. Many methods [MBLD02; Das03; JSWD05] have been proposed to produce Wachspress' coordinates inside a convex n-gon using different approaches. [WSHD07; DW08a; KB15; KB16] extended Wachspress method from a polygon to a convex closed curved bounded domain. However, the main limitation of Wachspress's method is the restriction to convex shapes. [MD04] replaced the area function with a positive edge-length based function for concave polygons, and [DW08b] provided an extension to concave shapes as well.

Mean value coordinates developed by [Flo03; HF06] works well on arbitrary closed polygons. Mean value coordinates are motivated by approximating a harmonic function over a polygon with the boundary fixed as a linear function along the polygon edges. These coordinates are well defined on the whole 2D plane for arbitrary non-intersecting polygons, which contrasts with Wachspress coordinates that are only defined on the interior of a convex polygon. [FKR05; JSW05] extended mean value coordinates to 3D for closed triangle meshes. [LS08] modified mean value coordinates to control derivatives at interpolated points. [APH17] blended mean value coordinates over Delaunay triangulation of the control polygon to generate local, closed form coordinates.

Floater [FHK06; Flo15] also developed a parameterized family of barycentric weights for convex polygons. This parameter, when chosen correctly, leads to Wachspress's coordinates, mean value coordinates, and discrete harmonic coordinates; though only the parameters for Wachspress and mean value coordinates led to positive coordinates for all convex polygons. [JLW07] extended this family of barycentric coordinate to 3D generalizing Wachspress coordinates, mean value coordinates, and discrete harmonic coordinates. [BLTD16] introduced a family of barycentric coordinates called Power Coordinates using a parameter function and included Wachspress, mean value coordinates and discrete harmonic coordinates as special cases as well.

Many other barycentric coordinates have been developed for planar polygons. Maximum Entropy Coordinates [HS08] utilize the Principle of Maximum Entropy to generate positive coordinates and work well for arbitrary polytopes inside the convex hull of the polytopes, though these coordinates require a nonlinear optimization at each evaluation point. [FH07] created a rational interpolant based on barycentric coordinates that produces no poles. [LLC08] introduced Green Coordinates for closed polyhedral cages and showed applications to 3D mesh deformation. [MS10] generated a family of barycentric coordinate for arbitrary polygons as well as polygons with boundary.

3. Review of the Floater-Hormann-Kós Family

Our approach generalizes the Floater-Hormann-Kós family of barycentric coordinates to non-convex shapes as well as shapes

with boundaries and into arbitrary dimension. Hence, we first begin with an in-depth review of the Floater-Hormann-Kós family of coordinates for 2D convex shapes.

Given a convex polygon with vertices $\{P_1, P_2, \dots, P_n\}$ and a point X with $P_i, X \in \mathbb{R}^2$, we consider each triangle formed by two consecutive edges P_{i-1}, P_i and P_i, P_{i+1} as shown in Figure 1. The authors construct their generalized barycentric coordinates di-

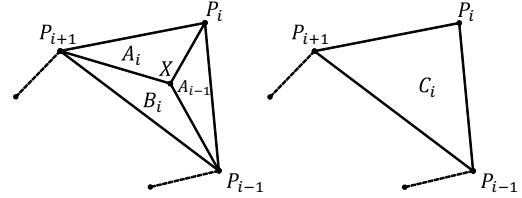


Figure 1: Triangulate a 2D polygon with point X.

rectly from the simplicial case of a triangle using the signed areas A_i, A_{i-1}, B_i formed by the edges of the triangle and point X as shown in the figure. Using Cramer's rule yields

$$A_i P_{i-1} + B_i P_i + A_{i-1} P_{i+1} = C_i X,$$

which can be rewritten as

$$A_i(P_{i-1} - X) + B_i(P_i - X) + A_{i-1}(P_{i+1} - X) = 0, \quad (3)$$

where $A_i + A_{i-1} + B_i = C_i$.

Equation 3 appears very similar to Equation 2, and indeed Equation 3 defines barycentric coordinates for the triangle with vertices P_{i-1}, P_i, P_{i+1} . To extend this equation to the entire polygon, the authors multiply Equation 3 by a non-negative function designed to create infinite weights along the two edges of the polygon touching P_i and sum over all triangles formed by two consecutive edges of the polygon. Such a function will force the boundary interpolation property when the homogeneous weights are renormalized.

In this case, the authors choose the parameterized function $\frac{c_i}{A_{i-1}A_i}$ where $c_i > 0$ are positive functions. Therefore,

$$\sum_{i=1}^n \frac{c_i}{A_{i-1}A_i} (A_i(P_{i-1} - X) + B_i(P_i - X) + A_{i-1}(P_{i+1} - X)) = 0.$$

If we reorder this summation to group terms by $(P_i - X)$, we obtain

$$\sum_{i=1}^n \frac{c_{i+1}A_{i-1} + c_i B_i + c_{i-1}A_i}{A_{i-1}A_i} (P_i - X) = 0.$$

This equation mirrors Equation 2 and gives the form of the homogeneous weight functions

$$w_i = \frac{c_{i+1}A_{i-1} + c_i B_i + c_{i-1}A_i}{A_{i-1}A_i}.$$

Summing these functions gives the denominator to create the normalized barycentric coordinates functions, which is

$$W = \sum_{i=1}^n w_i = \sum_{i=1}^n \frac{c_{i+1}A_{i-1} + c_i B_i + c_{i-1}A_i}{A_{i-1}A_i} = \sum_{i=1}^n \frac{c_i C_i}{A_{i-1}A_i}.$$

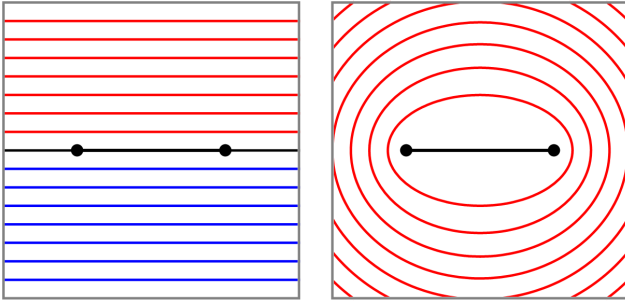


Figure 2: Given a line segment in 2D, A_i used in the Floater-Hormann-Kós family (left) defines a linear function that may be negative (blue) and whose zero level set extends outside the line segment. Our elliptical function (right) is always positive (red) except on the line segment itself where it is zero.

Note that, since C_i, A_i, A_{i-1} are positive for all X in a convex polygon and $c_i > 0$, then W is positive for all X and produces barycentric coordinate functions that have no poles within the domain of the convex polygon.

The parameters c_i can be arbitrary functions in this family of coordinates. Different choices produce different barycentric coordinates. The authors take $c_i = |P_i - X|^\alpha$. This choice of parameter reproduces several common barycentric coordinate constructions including Wachspress coordinates ($\alpha = 0$) and mean value coordinates ($\alpha = 1$).

4. Generalized 2D Barycentric Coordinates

The Floater-Hormann-Kós family of barycentric coordinates provides an infinite set of coordinates for convex shapes. However, the restriction to convex shapes is limiting. To generalize these coordinates, we must understand why the original family creates issues for non-convex polygons. There are two potential problems that arise when generalizing these coordinates. The first is the choice of weight function for blending the local barycentric coordinates from Equation 3. The original choice of weight function, $\frac{c_i}{A_{i-1}A_i}$, is positive and well-defined for convex polygons. However, the choice of using the areas, A_i , in the denominator produces poles and negative values on the interior of non-convex polygons.

The second difficulty appears in the normalization of the homogeneous coordinates. To be well-defined everywhere, the normalization factor $W = (\sum_{i=1}^n w_i)$ must be positive for all X . If this were not the case, the denominator would approach zero and create poles in the resulting basis functions.

To remedy these issues, we begin by replacing the $\frac{1}{A_i}$ in the weight function with $\frac{1}{d_i^\beta}$ where $\beta \geq 1$, which is a similar function that is positive everywhere except the edge of the polygon. β represents a parameter that controls the rate of fall off of the weight functions. We define

$$d_i = |P_i - X| + |P_{i+1} - X| - |P_{i+1} - P_i|. \quad (4)$$

d_i has the property that it is zero when X lies on the line segment from P_i to P_{i+1} (necessary to create the boundary interpolation property) but is positive for all other values of X . Figure 2 shows a plot of d_i versus A_i used in the Floater-Hormann-Kós family.

Our final weight function becomes

$$\frac{c_i \sin(\phi_i)}{(d_{i-1}d_i)^\beta} \quad (5)$$

where ϕ_i is the angle at P_i formed by the edges P_{i-1}, P_i , and P_{i+1} . We add the $\sin(\phi_i)$ term to guarantee that the basis functions will be well-defined everywhere as shown below.

Using Equation 3, we have

$$\sum_{i=1}^n \frac{c_i \sin \phi_i}{(d_i d_{i-1})^\beta} (A_i P_{i-1} + B_i P_i + A_{i-1} P_{i+1}) = WX \quad (6)$$

where W is the sum of the coefficients. Regrouping the terms by P_i yields

$$\sum_{i=1}^n w_i P_i = WX$$

where

$$w_i = \frac{c_{i-1} \sin \phi_{i-1} A_{i-2}}{(d_{i-2} d_{i-1})^\beta} + \frac{c_i \sin \phi_i B_i}{(d_{i-1} d_i)^\beta} + \frac{c_{i+1} \sin \phi_{i+1} A_{i+1}}{(d_i d_{i+1})^\beta} \quad (7)$$

gives our homogeneous barycentric weight functions.

Our barycentric coordinates are well-defined for both convex and non-convex polygons, which we demonstrate by computing the normalization, W , of the coordinates using the fact that $|P_i - P_{i-1}| |P_{i+1} - P_i| \sin \phi_i = 2C_i$ with Equation 6.

$$\begin{aligned} W &= \sum_{i=1}^n w_i \\ &= \sum_{i=1}^n \frac{c_i \sin \phi_i}{(d_i d_{i-1})^\beta} (A_i + B_i + A_{i-1}) \\ &= \sum_{i=1}^n \frac{2c_i C_i}{|P_i - P_{i-1}| |P_{i+1} - P_i| (d_i d_{i-1})^\beta} (A_i + B_i + A_{i-1}) \\ &= \sum_{i=1}^n \frac{2c_i C_i}{|P_i - P_{i-1}| |P_{i+1} - P_i| (d_i d_{i-1})^\beta} C_i \\ &= \sum_{i=1}^n \frac{2c_i C_i^2}{|P_i - P_{i-1}| |P_{i+1} - P_i| (d_i d_{i-1})^\beta} \end{aligned}$$

Since $c_i > 0$ and we require that the polygon is non-degenerate, then there exists a $C_i \neq 0$ and each term of the final summation of W is non-negative. Therefore W is positive everywhere. The $\{w_i\}$ also contain no singularities excluding the polygon boundary. Hence, the normalized barycentric coordinates are well defined for arbitrary polygons, convex or not. Note that, while the sum of the coordinate functions W is positive, there is no guarantee that the weight functions w_i will be positive in the interior of the polygon for non-convex shapes.

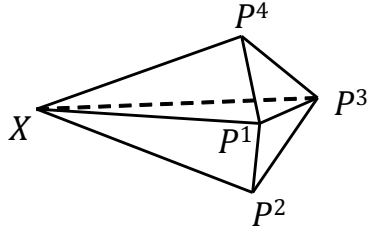


Figure 3: Two triangles sharing a common edge.

5. 3D Barycentric Coordinates

Extending this family of barycentric coordinates to 3D is relatively simple. A control polygon in 2D becomes a control mesh in 3D consisting of triangles. Instead of focusing on two line segments sharing a vertex, we instead consider two triangles sharing an edge. We need only to generalize our weight function in Equation 5 and use Cramer's rule in Equation 3. Referring to Figure 3, we define

$$V_i^j = \text{Vol}(P_i^1, \dots, P_i^{j-1}, X, P_i^{j+1}, \dots, P_i^4)$$

where Vol is the signed area/volume of the simplex formed by its arguments and P_i^j refers to the j^{th} vertex of the two triangles sharing the i^{th} edge in the control mesh. Note that the volume of the tetrahedra formed by the P_i^j is related to these quantities and is given by

$$\text{Vol}(P_i^1, P_i^2, P_i^3, P_i^4) = \sum_{j=1}^4 V_i^j.$$

In 3D, the generalization of Equation 3 then becomes

$$V_i^1(P_i^1 - X) + V_i^2(P_i^2 - X) + V_i^3(P_i^3 - X) + V_i^4(P_i^4 - X) = 0. \quad (8)$$

To generalize Equation 5, we first generalize the d_i^1, d_i^2 to higher dimension using triangle areas where d_i^1 corresponds to the first triangle sharing the i^{th} edge and d_i^2 the second triangle.

$$\begin{aligned} d_i^1 &= |\text{Vol}(X, P_i^1, P_i^2)| + |\text{Vol}(X, P_i^2, P_i^3)| \\ &\quad + |\text{Vol}(X, P_i^3, P_i^1)| - |\text{Vol}(P_i^3, P_i^2, P_i^1)| \\ d_i^2 &= |\text{Vol}(X, P_i^1, P_i^3)| + |\text{Vol}(X, P_i^3, P_i^4)| \\ &\quad + |\text{Vol}(X, P_i^4, P_i^1)| - |\text{Vol}(P_i^4, P_i^3, P_i^1)| \end{aligned}$$

Like Equation 4, these values are positive everywhere except at the corresponding triangle where the function is zero. Now we generalize the $\sin \phi_i$ term by defining ϕ_i to be the dihedral angle between the two polygons sharing the edge i . Note that the sine of this angle has a simple form [GL96]

$$\sin \phi_i = \frac{3}{2} \frac{\text{Vol}(P_i^1, P_i^2, P_i^3, P_i^4) \|P_i^1 - P_i^3\|}{|\text{Vol}(P_i^1, P_i^2, P_i^3)| |\text{Vol}(P_i^1, P_i^3, P_i^4)|}. \quad (9)$$

Combining Equation 8 with our weight function yields

$$\sum_i \frac{c_i \sin \phi_i}{(d_i^1 d_i^2)^\beta} (V_i^1 P_i^1 + V_i^2 P_i^2 + V_i^3 P_i^3 + V_i^4 P_i^4) = WX \quad (10)$$

where i iterates over the edges in the control mesh. As in 2D, we require that $c_i > 0$. Re-indexing this summation over the vertices of

the control mesh provides the homogeneous form of the barycentric weight functions for each vertex.

$$w_P = \sum_{i \in I} \frac{c_i \sin \phi_i}{(d_i^1 d_i^2)^\beta} V_i^j \quad (11)$$

where the indices set $I = \{i | \exists j \text{ s.t. } P_i^j = P\}$ is all the tetrahedrons containing vertex P .

To show that our homogeneous weights are well defined everywhere, we note that our weight function $\frac{c_i \sin \phi_i}{(d_i^1 d_i^2)^\beta}$ has no poles anywhere except at the triangles of the control mesh. We then simply need to show that the normalization factor for these weight functions W is always non-zero. The sum of these weight function is given by

$$W = \sum_P w_P = \sum_i \frac{c_i \sin \phi_i}{(d_i^1 d_i^2)^\beta} \text{Vol}(P_i^1, P_i^2, P_i^3, P_i^4)$$

Substituting Equation 9 into this sum yields

$$W = \sum_i \frac{3}{2} \frac{c_i \text{Vol}(P_i^1, P_i^2, P_i^3, P_i^4) \|P_i^1 - P_i^3\|}{(d_i^1 d_i^2)^\beta |\text{Vol}(P_i^1, P_i^2, P_i^3)| |\text{Vol}(P_i^1, P_i^3, P_i^4)|}.$$

All of the quantities in the sum are non-negative everywhere. Therefore, W is always positive and the W_P are well-defined everywhere for non-degenerate shapes.

5.1. Higher Dimensions

The generalization to 3D barycentric coordinates in Section 5 gives a path to extend these coordinates to arbitrary dimensions. Our coordinates generalize to meshes of co-dimension 1 with vertices in \mathbb{R}^n whose facets are $(n-1)$ -dimensional simplices. Given two adjacent $(n-1)$ -dimensional facets, f_i^1 and f_i^2 with vertices $P_i^1 \dots P_i^{n-1}$ and $P_i^2 \dots P_i^n$ respectively, the union of these facets forms an n -simplex $f_i^1 \cup f_i^2$, and their intersection $f_i^1 \cap f_i^2$ forms the i^{th} $(n-2)$ -simplex of the control mesh.

The linear reproduction property can be written as

$$\sum_{j=1}^n \text{Vol}(P_i^1, \dots, P_i^{j-1}, X, P_i^{j+1}, \dots, P_i^n) (P_i^j - X) = 0.$$

We utilize the same weight function $\frac{c_i \sin \phi_i}{(d_i^1 d_i^2)^\beta}$ where ϕ_i is the dihedral angle between f_i^1 and f_i^2 . Fortunately, the sine of the dihedral angle between two adjacent simplices has a simple expression in high dimensions [GL96].

$$\sin \phi_i = \kappa \frac{\text{Vol}(f_i^1 \cup f_i^2) |\text{Vol}(f_i^1 \cap f_i^2)|}{|\text{Vol}(f_i^1)| |\text{Vol}(f_i^2)|}$$

κ is a constant that only depends on the dimension n . However, since the weights are in homogeneous form, we can ignore constant factors. d_i^1 and d_i^2 then become

$$\begin{aligned} d_i^1 &= \sum_{j=1}^{n-1} \left| \text{Vol}(P_i^1, \dots, P_i^{j-1}, X, P_i^{j+1}, \dots, P_i^{n-1}) \right| - |\text{Vol}(f_i^1)| \\ d_i^2 &= \sum_{j=2}^n \left| \text{Vol}(P_i^2, \dots, P_i^{j-1}, X, P_i^{j+1}, \dots, P_i^n) \right| - |\text{Vol}(f_i^2)|. \end{aligned} \quad (12)$$

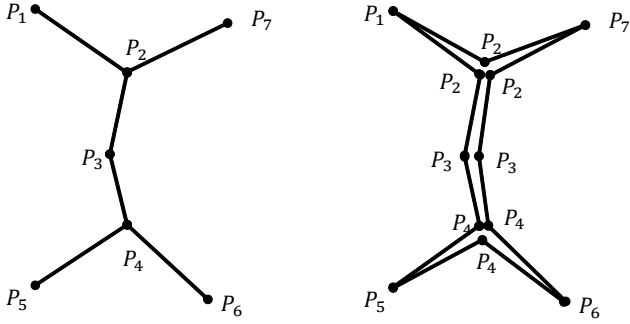


Figure 4: A control skeleton for barycentric coordinates (left), and its representation as a closed polygon (right).

Combining our weight function

$$\frac{c_i \sin \phi_i}{(d_i^1 d_i^2)^\beta}$$

with Equation 12 and re-indexing over the vertices yields barycentric coordinates over this simplicial complex.

$$w_P = \sum_{i \in I} \frac{c_i \sin \phi_i}{(d_i^1 d_i^2)^\beta} V_i^j \quad (13)$$

where the indices set $I = \{i | \exists j \text{ s.t. } P_i^j = P\}$ is all the simplices containing vertex P .

The sum of the weights W is the normalization factor, which is given by

$$W = \sum_i \frac{c^i \sin \phi^i \text{Vol}(f_i^1 \cup f_i^2)}{(d_i^1 d_i^2)^\beta} = \sum_i \frac{c^i \text{Vol}(f_i^1 \cup f_i^2)^2 |V(f_i^1 \cap f_i^2)|}{(d_i^1 d_i^2)^\beta |V(f_i^1)| |V(f_i^2)|} > 0,$$

which is always positive. Therefore, these coordinates are well defined everywhere. In addition, our basis functions reduce down to the lower dimensional barycentric basis functions along the boundary of the control shape and satisfy the “interpolation” property described in Section 1.

6. Non-Manifold Shapes

Our family of barycentric coordinates not only extends to higher dimensional shapes and is well-defined everywhere but can be extended to non-manifold shapes or shapes with boundaries. This is in contrast to barycentric coordinate constructions like mean value coordinates [Flo03] that require closed shapes to guarantee linear precision in the resulting coordinate functions. We demonstrate such an extension for 2D and for 3D, though the technique generalizes to arbitrary dimension.

6.1. Barycentric Coordinates for 2D Skeletons

2D skeletons can be considered as a special case of a closed polygon. Consider the skeleton in Figure 4 (left) where the topology

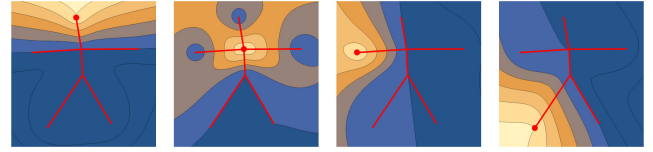


Figure 5: Example basis functions of a skeleton control shape with $c_i = 1$ and $\beta = 1$.

of the shape is a connected tree. We can treat the tree as a degenerate closed polygon by traversing the outside of the boundary. In this example, such a path produces the sequence of vertices “ $P_1, P_2, P_7, P_2, P_3, P_4, P_6, P_4, P_5, P_4, P_3, P_2$ ” that represents a degenerate, but closed, polygon shown in Figure 4 (right). Applying our construction from Equation 7 yields valid barycentric coordinates. Figure 5 shows an example of several barycentric basis functions constructed from a skeleton control shape using our method.

While the generality of handling skeletons is appealing, we should note that some vertices may end up with barycentric basis functions that are identically zero. All vertices on a straight line are not valid input data. In the other word, the vertices must span 2D space, because barycentric coordinates only exist in the sub space spanned by the input vertices. However, it is possible that three or more vertices are colinear. If only three vertices are colinear, our coordinates maintain constant and linear precision as well as the interpolation property along the edges. When four or more consecutive vertices are colinear, some of the w_i may be identically zero. Specifically, if $m + 1$ vertices P_k through P_{m+k} are connected in sequence and colinear, then w_{k+2} through w_{m+k-2} will be zero. In all cases, our coordinates maintain constant and linear precision and are well-defined everywhere despite the inclusion of identically zero w_i . Compared with Wachspress coordinates [Wac75] where the w_{k+1} through w_{m+k-1} would be zero, our coordinate construction produces fewer identically zero basis functions. However, our coordinates lose the interpolation property on the edges formed by the vertices P_{k+1} through P_{m+k-1} .

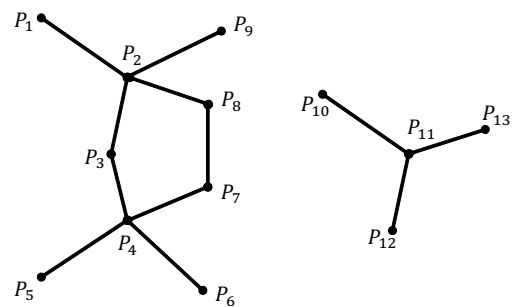


Figure 6: An example 2D control shape of arbitrary topology consisting of two disjoint components.

6.2. Arbitrary Topology in 2D

Our method extends beyond trees in 2D to arbitrary topology as well. For example, Figure 6 consists of two separate control shapes,

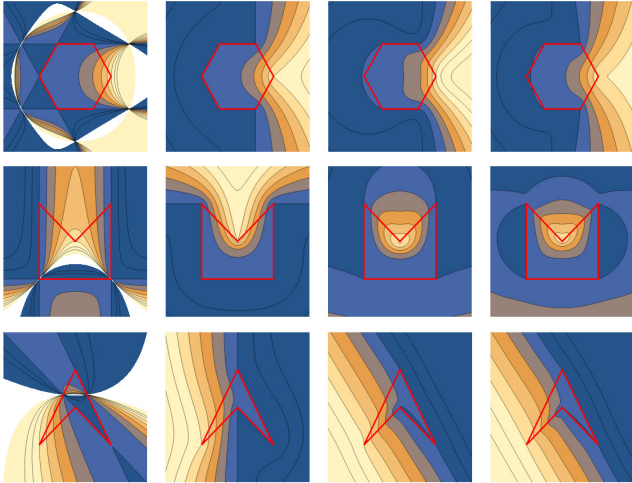


Figure 7: Barycentric basis functions of different control polygons. From left to right: Wachspress $c_i = 1$, mean Value $c_i = \|P_i - X\|$, our method $c_i = 1$, our method $c_i = \|P_i - X\|$. $\beta = 1$ in all examples.

one of which contains a cycle. In this case, we simply process every triple of consecutive vertices in the summation from Equation 6 to create barycentric coordinates. Equation 6 does not require the shape to be closed or that the shape is even connected. Instead, the equation will build local, homogeneous barycentric coordinates for any two line segments sharing a vertex. Hence, we only need a cyclic ordering of vertices around each vertex to create all consecutive line segments sharing a vertex. For example, the set of line segments sharing P_4 are (P_3, P_4, P_5) , (P_5, P_4, P_6) , (P_6, P_4, P_7) , and (P_7, P_4, P_3) . Rewriting the summation in Equation 6 over the vertices of the shape yields barycentric coordinates for this general control shape.

6.3. Barycentric Coordinates for 3D Sheets

In 3D, our method generalizes to arbitrary triangle meshes as well. In this case, we iterate over pairs of triangles sharing a common edge and evaluate Equation 10. Doing so allows us to handle meshes that have boundaries or even form skeletal sheet-like structures. Note that our method requires surfaces of co-dimension 1. So true 3D skeletons consisting of line segments cannot be handled by our method. However, 3D skeletons consisting of triangles forming a median sheet can. Figure 11 shows an example of such a sheet controlling the deformation of a 3D surface.

6.4. Higher Dimensions

For dimension ≥ 4 , our mirrors the lower dimensional constructions. We iterate through all $(n - 2)$ -dimensional simplices part of the control polytope that are the intersection between two adjacent $(n - 1)$ -dimensional simplices of the control polytope. The equations in Section 5.1 apply to these pairs whether or not the control polytope forms a closed manifold or not.

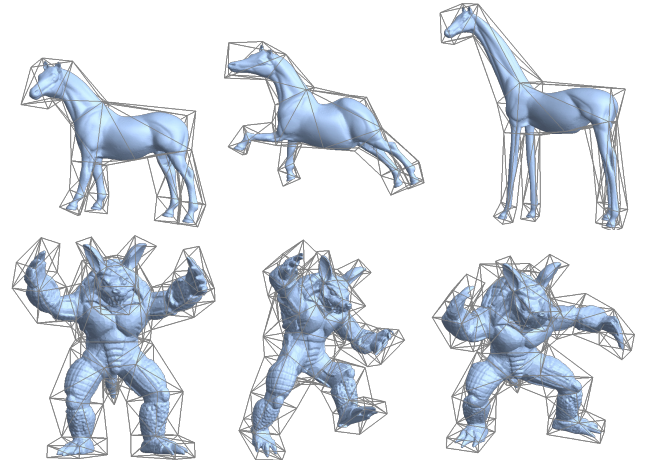


Figure 8: Deformation of the initial 3D mesh (left) using our barycentric coordinates (middle/right) with $c_i = 1$ and $\beta = 1$.

7. Results

We compare our family of barycentric coordinates with the Floater-Hormann-Kós family of barycentric coordinates in Figure 7. This figure shows three different control polygons, one in each row consisting of a convex control polygon (top) and two different concave control polygons. We show a single barycentric basis function corresponding to the same vertex in each row. The first two columns show Wachspress coordinates ($c_i = 1$) [Wac75; FHK06] and mean value coordinates ($c_i = \|P_i - X\|$) [Flo03; FHK06]. The next two columns show our coordinates with the same c_i values and $\beta = 1$.

For convex shapes, each of the four basis functions are well defined within the interior of the control polygon. However, Wachspress coordinates contain poles along a curve surrounding the control polygon, which is shown as a white region due to the limited number of levels sets shown in the figure. Mean value coordinates as well as our coordinates are well-defined everywhere and yield similar, although not identical, basis functions.

For concave shapes, the results are quite different. Wachspress coordinates contain poles that extend to the interior. However, the other coordinates do not contain such poles, but also appear different particularly on the outside of the control polygon.

In 3D, the basis functions are much more difficult to visualize. However, we can use the barycentric coordinates for cage-based deformations as defined by [JSW05] to visualize the effect of the basis functions. As shown in Figure 8, we begin with a low-resolution control cage with a high-resolution shape (Figure 8 left). We compute the barycentric coordinates of each high-resolution vertex as a weighted combination of the low-resolution control cage. Deforming the control cage then induces a deformation of the high-resolution shape. Figure 8 right shows several example deformations using our method with $c_i = 1$ and $\beta = 1$.

Our barycentric coordinates can also be used with more arbitrary control shapes such as the skeleton shown in Figure 9. Despite not being a closed polygon, our method can still construct barycentric coordinates for the entire 2D plane. Figure 9 middle and right

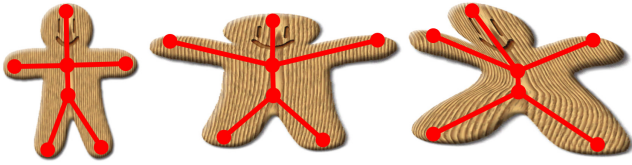


Figure 9: 2D deformation using a general control shape with $c_i=1$ and $\beta=1$.

shows two deformed shapes generated by moving the vertices of the skeleton with $c_i = 1$ and $\beta = 1$.

Figure 10 shows a similar example to Figure 9 comparing our deformation to that generated by mean value coordinates [FHK06]. While Section 6.1 showed how we could consider such control shapes as collapsed polygons, mean value coordinates produce zero coordinates for all of the regions with zero area. The inclusion of the triangle on the head prevents the entirely degenerate case of mean value coordinates with all coordinates being zero. However, in this example, all 2D points for mean value coordinates are defined by the three vertices of the triangle. Hence, when we move the arms and legs (Figure 10 middle), nothing changes. In contrast, our method (Figure 10 right) interpolates all of the edges and produces a deformation regardless of the control shape.

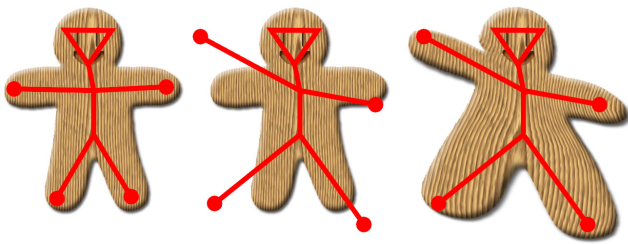


Figure 10: Deformation of the initial shape (left) with our coordinates with $c_i = 1$ and $\beta = 1$ (right) produces a natural deformation. However, mean value coordinates (middle) cannot operate on such generate shapes and produces no deformation.

The corresponding example in 3D is not a 1D skeleton but a 2D sheet. Figure 11 shows such an example where we approximate the skeleton of the armadillo man with a sheet having several non-manifold edges. Our method creates a realistic deformation of the shape in the middle figure using a skeleton-like control as shown in the figure with $c_i = 1$ and $\beta = 2$. Note that our method deforms the ambient space rather than space specific to the object being deformed like the arms or legs of the armadillo man. While all points are influenced by all others, β controls the rate of fall off, which we use to manipulate the region of influence in practice. However, extreme deformations may cause unwanted artifacts such as unwanted sheering as shown in the leg in Figure 11 (right).

β is a shape parameter for the barycentric basis functions in our method. Figure 12 shows an example of a 2D deformation where we expand the bottom and shrink the top of the figure. After the initial figure, we show the same deformed control polyline with

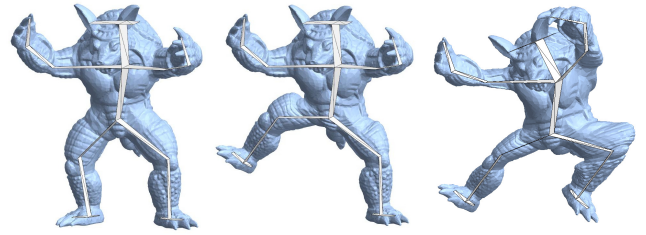


Figure 11: Deformation of an armadillo man by deforming a zero volume 3D skeleton with $c_i = 1$ and $\beta = 2$. The right image shows a more extreme deformation with sheering artifacts.

$c_i = 1$ but modify β and use $\beta = 1, 1.5, 2$. As β increases, so too does the locality of the deformation in the region around each edge. In the figure, this effect manifests itself in the enlargement of the body near the feet and the shrinking of the horns in the figure. Lower values of β tend to produce less locality and more averaging of the deformation over space.

Our barycentric coordinate construction generalizes many prior constructions to arbitrary shapes allowing for control shapes not possible in the Floater-Hormann-Kós family. While we visualize these basis functions through deformation applications, there are many applications of barycentric coordinates, and our functions were not designed specifically to create pleasing deformations. For animation applications, minimizing variational properties such as the first derivative as in Harmonic Coordinates [JMD*07] or second derivative to create weight functions as in Bounded Biharmonic Coordinates [JBPS11] will likely produce higher quality results though those basis functions are more computationally intensive to evaluate.

Our basis functions also exhibit an averaging effect outside the control shape for very concave control shapes. Figure 13 shows an example of a very concave shape with Wachspress coordinates, mean value coordinates, and our method for the concave inner vertex. Wachspress coordinates produce poles where the basis functions are undefined. However, our method differs from mean value coordinates in that the basis function for the inner vertex appears more like a linear function with a local deviation around the polygon. This behavior can produce unintuitive deformations in some cases. Figure 14 shows examples of three different control polygons (left) followed by a deformation from mean value coordinates (middle) and our method (right). For convex shapes, the resulting deformations are similar. However, concave shapes show more deviation. In the middle example, the outside of the image is more



Figure 12: From left to right: the initial shape/control polyline and our deformed shape with $c_i=1$ and $\beta = 1, 1.5,$ and 2 .

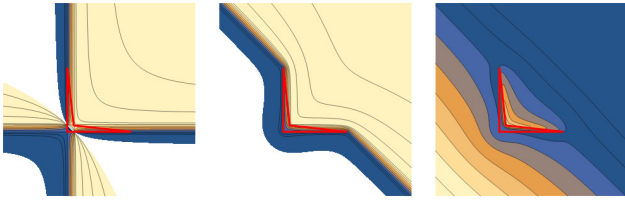


Figure 13: Basis functions of the inner concave vertex for a nearly degenerate shape using Wachspress coordinates (left), mean value coordinates (center), and our method with $c_i = 1$ and $\beta = 1$ (right).

strongly compressed as opposed to exaggerated with mean value coordinates under deformation. The bottom shows a deformation with the control polygon from Figure 13. Expanding the vertex outward actually leads to a compression effect with our method and the image folds on itself. However, mean value coordinates produces a strong non-uniform scaling effect for the same movement of the control polygon.

Floater et al. [FK10] also explored the injectivity of Wachspress and mean value coordinates when used for deformations from a convex polygon to another convex polygon. The lack of injectivity can lead to folds in the deformed shapes that can be undesirable. The authors showed that only Wachspress coordinates guaranteed injective deformations in this highly restrictive manner. While we have not investigated the injectivity of our deformations in this setting, our deformations certainly have no guarantee of injectivity with concave control shapes. Figures 14 (bottom right) and 11 (right) show examples of extreme deformations where our method does not produce pleasing results. It may be possible to choose the c_i or β parameters to minimize variational quantities in our method, but we have not explored this avenue.

8. Conclusions and Limitations

Our work generalizes the Floater-Hormann-Kós family of barycentric coordinates from convex 2D shapes to arbitrary poly-lines and into arbitrary dimension. Our coordinates are well-defined not only within the control polygon but everywhere. To do so, we required only small modifications to the weight function used in the original construction.

As to limitations, our method requires that the boundary faces of the control shape be simplices. In 2D, this limitation is trivially satisfied. However, in 3D, this requirement means that control shapes must be triangle meshes (or the equivalent in higher dimensions). In addition, our method cannot handle completely arbitrary topology shapes. For example, in 2D we require that two line segments share a vertex, which precludes using soups of line segments without any connectivity.

Acknowledgements

This work was funded in part by gifts from Adobe and Activision.

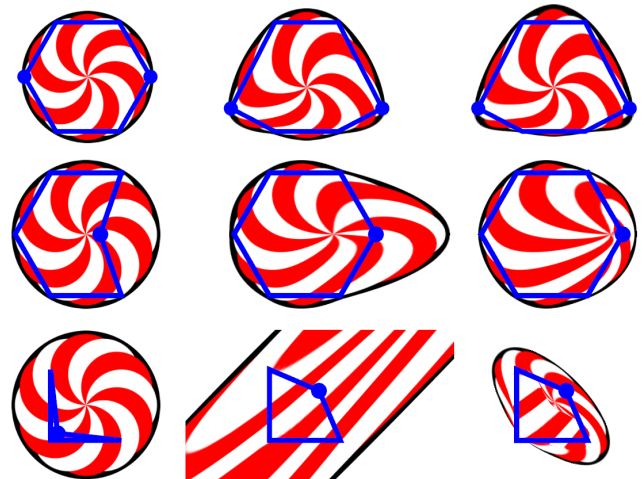


Figure 14: Three different deformations comparing our method with $c_i = 1$ and $\beta = 1$ and mean value coordinates. Left to right: original shape, deformation with mean value coordinates, our method.

References

- [APH17] ANISIMOV, DMITRY, PANOZZO, DANIELE, and HORMANN, KAI. “Blended barycentric coordinates”. *Computer Aided Geometric Design* 52 (2017), 205–216 2.
- [BLTD16] BUDNINSKIY, MAX, LIU, BEIBEI, TONG, YIYING, and DESBRUN, MATHIEU. “Power coordinates: a geometric construction of barycentric coordinates on convex polytopes”. *ACM Transactions on Graphics (TOG)* 35.6 (2016), 241 2.
- [Das03] DASGUPTA, GAUTAM. “Interpolants within convex polygons: Wachspress’ shape functions”. *Journal of Aerospace Engineering* 16.1 (2003), 1–8 2.
- [DW08a] DASGUPTA, GAUTAM and WACHSPRESS, E. “The adjoint for an algebraic finite element”. *Computers & Mathematics with Applications* 55.9 (2008), 1988–1997 2.
- [DW08b] DASGUPTA, GAUTAM and WACHSPRESS, EUGENE L. “Basis functions for concave polygons”. *Computers & Mathematics with Applications* 56.2 (2008), 459–468 2.
- [FH05] FLOATER, MICHAEL S and HORMANN, KAI. “Surface parameterization: a tutorial and survey”. *Advances in multiresolution for geometric modelling*. Springer, 2005, 157–186 1.
- [FH07] FLOATER, MICHAEL S and HORMANN, KAI. “Barycentric rational interpolation with no poles and high rates of approximation”. *Numerische Mathematik* 107.2 (2007), 315–331 2.
- [FHK06] FLOATER, MICHAEL S, HORMANN, KAI, and KÓS, GÉZA. “A general construction of barycentric coordinates over convex polygons”. *Advances in computational mathematics* 24.1-4 (2006), 311–331 1, 2, 6, 7.
- [FHL*09] FARBMAN, ZEEV, HOFFER, GIL, LIPMAN, YARON, et al. “Coordinates for instant image cloning”. *ACM Transactions on Graphics (TOG)*. Vol. 28. 3. ACM. 2009, 67 1.
- [FK10] FLOATER, MICHAEL S. and KOSINKA, JIŘÍ. “On the injectivity of Wachspress and mean value mappings between convex polygons”. *Advances in Computational Mathematics* 32.2 (2010), 163–174 8.
- [FKR05] FLOATER, MICHAEL S, KÓS, GÉZA, and REIMERS, MARTIN. “Mean value coordinates in 3D”. *Computer Aided Geometric Design* 22.7 (2005), 623–631 2.

- [Flo03] FLOATER, MICHAEL S. “Mean value coordinates”. *Computer aided geometric design* 20.1 (2003), 19–27 [2](#), [5](#), [6](#).
- [Flo15] FLOATER, MICHAEL S. “Generalized barycentric coordinates and applications”. *Acta Numerica* 24 (2015), 161–214 [1](#), [2](#).
- [FS08] FLOATER, MICHAEL S and SCHULZ, CHRISTIAN. “Pointwise radial minimization: Hermite interpolation on arbitrary domains”. *Computer Graphics Forum*. Vol. 27. 5. Wiley Online Library. 2008, 1505–1512 [1](#).
- [GL96] GANGSONG, LENG and LIHUA, TANG. “Some inequalities on the inradii of a simplex and of its faces”. *Geometriae Dedicata* 61.1 (1996), 43–49 [4](#).
- [HF06] HORMANN, KAI and FLOATER, MICHAEL S. “Mean value coordinates for arbitrary planar polygons”. *ACM Transactions on Graphics (TOG)* 25.4 (2006), 1424–1441 [2](#).
- [HS08] HORMANN, KAI and SUKUMAR, NATARAJAN. “Maximum entropy coordinates for arbitrary polytopes”. 27.5 (2008), 1513–1520 [2](#).
- [JBPS11] JACOBSON, ALEC, BARAN, ILYA, POPOVIC, JOVAN, and SORKINE, OLGA. “Bounded biharmonic weights for real-time deformation.” *ACM Trans. Graph.* 30.4 (2011), 78–1 [7](#).
- [JLW07] JU, TAO, LIEPA, PETER, and WARREN, JOE. “A general geometric construction of coordinates in a convex simplicial polytope”. *Computer Aided Geometric Design* 24.3 (2007), 161–178 [2](#).
- [JMD*07] JOSHI, PUSHKAR, MEYER, MARK, DEROSE, TONY, et al. “Harmonic Coordinates for Character Articulation”. *ACM Trans. Graph.* 26.3 (2007) [7](#).
- [JSW05] JU, TAO, SCHAEFER, SCOTT, and WARREN, JOE. “Mean value coordinates for closed triangular meshes”. 24.3 (2005), 561–566 [2](#), [6](#).
- [JSWD05] JU, TAO, SCHAEFER, SCOTT, WARREN, JOE D, and DESBRUN, MATHIEU. “A Geometric Construction of Coordinates for Convex Polyhedra using Polar Duals.” *Symposium on Geometry Processing*. 2005, 181–186 [1](#), [2](#).
- [KB15] KOSINKA, JIŘÍ and BARTOŇ, MICHAEL. “Convergence of Wachspress coordinates: from polygons to curved domains”. *Advances in Computational Mathematics* 41.3 (2015), 489–505 [2](#).
- [KB16] KOSINKA, JIŘÍ and BARTOŇ, MICHAEL. “Convergence of barycentric coordinates to barycentric kernels”. *Computer Aided Geometric Design* 43 (2016), 200–210 [2](#).
- [LKCL07] LIPMAN, YARON, KOPF, JOHANNES, COHEN-OR, DANIEL, and LEVIN, DAVID. “GPU-assisted positive mean value coordinates for mesh deformations”. *Symposium on geometry processing*. 2007 [1](#).
- [LLC08] LIPMAN, YARON, LEVIN, DAVID, and COHEN-OR, DANIEL. “Green coordinates”. *ACM Transactions on Graphics (TOG)* 27.3 (2008), 78 [2](#).
- [LS08] LANGER, TORSTEN and SEIDEL, HANS-PETER. “Higher order barycentric coordinates”. *Computer Graphics Forum*. Vol. 27. 2. Wiley Online Library. 2008, 459–466 [2](#).
- [MBLD02] MEYER, MARK, BARR, ALAN, LEE, HAEYOUNG, and DESBRUN, MATHIEU. “Generalized barycentric coordinates on irregular polygons”. *Journal of graphics tools* 7.1 (2002), 13–22 [2](#).
- [MD04] MALSCH, ELISABETH ANNA and DASGUPTA, GAUTAM. “Algebraic construction of smooth interpolants on polygonal domains”. *Mathematica Journal* 9.3 (2004), 641–658 [1](#), [2](#).
- [MJBFO2] MILLIRON, TIM, JENSEN, ROBERT J, BARZEL, RONEN, and FINKELSTEIN, ADAM. “A framework for geometric warps and deformations”. *ACM Transactions on Graphics (TOG)* 21.1 (2002), 20–51 [1](#).
- [MS10] MANSON, JOSIAH and SCHAEFER, SCOTT. “Moving least squares coordinates”. *Computer Graphics Forum*. Vol. 29. 5. Wiley Online Library. 2010, 1517–1524 [2](#).
- [SM06] SUKUMAR, N and MALSCH, EA. “Recent advances in the construction of polygonal finite element interpolants”. *Archives of Computational Methods in Engineering* 13.1 (2006), 129 [1](#).
- [Wac11] WACHSPRESS, EUGENE L. “Barycentric coordinates for polytopes”. *Computers & Mathematics with Applications* 61.11 (2011), 3319–3321 [2](#).
- [Wac75] WACHSPRESS, EUGENE L. *A rational finite element basis*. Academic Press, 1975 [1](#), [2](#), [5](#), [6](#).
- [Wac81] WACHSPRESS, EL. “High-order curved finite elements”. *International Journal for Numerical Methods in Engineering* 17.5 (1981), 735–745 [1](#).
- [War03] WARREN, JOE. “On the uniqueness of barycentric coordinates”. *Contemporary Mathematics* 334 (2003), 93–100 [2](#).
- [War96] WARREN, JOE. “Barycentric coordinates for convex polytopes”. *Advances in Computational Mathematics* 6.1 (1996), 97–108 [2](#).
- [WShD07] WARREN, JOE, SCHAEFER, SCOTT, HIRANI, ANIL N, and DESBRUN, MATHIEU. “Barycentric coordinates for convex sets”. *Advances in computational mathematics* 27.3 (2007), 319–338 [2](#).
- [ZDL*14] ZHANG, JUYONG, DENG, BAILIN, LIU, ZISHUN, et al. “Local barycentric coordinates”. *ACM Transactions on Graphics (TOG)* 33.6 (2014), 188 [1](#).